AGU PUBLICATIONS

Geophysical Research Letters

RESEARCH LETTER
10.1002/2016GL068721

Key Points:
- Circumferential dikes in calderas may be due to the caldera formation unloading
- The amount of dike deflection depends on the ratio between overpressure and unloading
- Progressive buoyancy increase is required to develop circumferential fissures

Supporting Information:
- Supporting Information S1

Correspondence to:
F. Corbi,
fabio.corbi3@gmail.com

Citation:
Corbi, F., E. Rivalta, V. Pinel, F. Maccaferri, and V. Acocella (2016), Understanding the link between circumferential dikes and eruptive fissures around calderas based on numerical and analog models, *Geophys. Res. Lett.*, *43*, doi:10.1002/2016GL068721.

Received 5 NOV 2015
Accepted 3 JUN 2016
Accepted article online 7 JUN 2016

Understanding the link between circumferential dikes and eruptive fissures around calderas based on numerical and analog models

Fabio Corbi[1], Eleonora Rivalta[1], Virginie Pinel[2], Francesco Maccaferri[1], and Valerio Acocella[3]

[1]GFZ German Centre for Geosciences, Section 2.1, Telegrafenberg, Germany, [2]ISTerre, Université Savoie Mont-Blanc, IRD, CNRS, Campus Scientifique, Le Bourget du Lac, France, [3]Dipartimento di Scienze, Università Roma Tre, Rome, Italy

Abstract Active calderas are seldom associated with circumferential eruptive fissures, but eroded magmatic complexes reveal widespread circumferential dikes. This suggests that, while the conditions to emplace circumferential dikes are easily met, mechanisms must prevent them from reaching the surface. We explain this discrepancy with experiments of air injection into gelatin shaped as a volcano with caldera. Analog dikes show variable deflection, depending on the competition between overpressure, P_e, and topographic unloading, P_l; when $P_l/P_e = 4.8–5.3$, the dikes propagate orthogonal to the least compressive stress. Due to the unloading, they become circumferential and stall below the caldera rim; buoyancy is fundamental for the further rise and circumferential fissure development. Numerical models quantitatively constrain the stress orientation within the gelatin, explaining the observed circumferential dikes. Our results explain how dikes propagate below the rim of felsic and mafic calderas, but only in the latter they are prone to feed circumferential fissures.

1. Introduction

Circumferential dikes are a common feature of many eroded and extinct volcanoes and magmatic complexes, as observed for example in Scotland [e.g., *Burchardt et al.*, 2013], the Canary Islands [e.g., *Ancochea et al.*, 2003], and Iceland [e.g., *Burchardt and Gudmundsson*, 2009]. Typically, these dikes are found at a depth of a few kilometers above the former magma chamber of the volcano. However, their surface expression as circumferential fissures is much more rare and specific of active volcanoes with a caldera (e.g., the western Galapagos Islands [*Acocella and Neri*, 2009, and references therein]). This suggests that the presence of a caldera may contribute significantly to the stress budget of a volcano influencing the location and orientation of the eruptive fissures. The conditions to develop circumferential dikes remain poorly constrained and, mostly, debated. In fact, at least three differing mechanisms may explain the creation of circumferential dikes: (1) viscous-dominated shallow intrusion into poorly consolidated rock [*Galland et al.*, 2014]; (2) fracturing-dominated or viscous-dominated intrusion into cohesive, brittle rock in presence of a radially oriented minimum compressional stress σ_3 possibly due to magma chamber stress [*Chadwick and Dieterich*, 1995; *Chestler and Grosfils*, 2013]; and (3) passive occupation of ring faults created during caldera collapse (not discussed here, see instead *Anderson* [1951], *Gudmundsson* [2006], and *Browning and Gudmundsson* [2015]). In addition, recent studies also revealed the importance of surface load changes in controlling shallow magma transfer. In fact, both analog and numerical models demonstrated that loading (or equivalently unloading) on the model surface may influence the principal stress orientation within a volcano and exert a strong control on dike propagation [e.g., *Fiske and Jackson*, 1972; *Dahm*, 2000; *Pinel and Jaupart*, 2000; *Acocella and Tibaldi*, 2005; *Watanabe et al.*, 2002; *Maccaferri et al.*, 2011; *Roman and Jaupart*, 2014; *Sigmundsson et al.*, 2015]. The loading or unloading may have different origin, such as ice cap melting [*Hooper et al.*, 2011], rifting [*Maccaferri et al.*, 2014], and fault scarps [*Maccaferri et al.*, 2015]. Here we further explore this mechanism, focusing on the effect due to the presence of a caldera, linking the circumferential dikes and fissures observed at proximal distance from the rim to the radially oriented σ_3 pattern that is caused by the creation of the topographic depression [*Corbi et al.*, 2015].

To this aim, we use analog models to test how the presence of a caldera controls the dike propagation and spatial arrangement. In these experiments, dike propagation is observed as a spontaneous and progressive process occurring in response to buoyancy force and external stresses. We inject air-filled cracks (dike analogs) into a cylindrical gelatin block (analog of cohesive rock), whose topography has been molded as a volcano with summit caldera. We also use a finite element approach to calculate numerically the state of

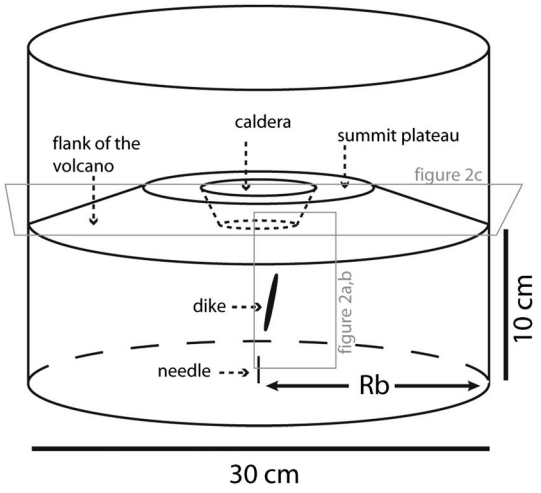

Figure 1. Sketch of the experimental setup. The gray rectangles highlight the area shown in Figure 2.

stress in the gelatin. Based on our results and on the comparison between experimental and numerical models, we discuss the validity of gelatin experiments for the investigation of dike trajectories, the kinematics of dike ascent, and the conditions to develop circumferential fissures.

2. Experimental Setup and Scaling

The experiments are prepared by pouring a 2 wt % type A (Italgelatine, S.p.A.) gelatin solution in a 30 cm diameter cylindrical Plexiglas® container. A shaping mold mimicking the morphology of a volcano with summit caldera is placed on the gelatin surface when the gelatin is in sol state (i.e., fluid-like). The radii of the inner and outer caldera rims are 2.5 cm and 4.25 cm, respectively. The summit plateau, simulating the outer caldera rim, is 2 cm wide and has an elevation of 4.5 cm with respect to the caldera floor. The slope of the outer flanks is ~30°. The solution is successively cooled in a refrigerator at 10 °C for 15 h, and the shaping mold is removed before running the experiment. The experiments are monitored from side and top view using two cameras with a frame rate of 0.2 Hz (Figure 1). Images are first corrected for the optical distortion due to the cylindrical container recovering a reference checkerboard inserted within the gelatin container. Then, the path of the propagating dike is tracked, identifying the position of the crack tip in each frame.

The gelatin shear modulus G depends on several factors including composition, concentration, and aging [*Di Giuseppe et al.*, 2009; *Kavanagh et al.*, 2013]. Under the applied experimental conditions $G = 580 \pm 30$ Pa, as measured through rheometer tests (Anton Paar, MCR301), the fracture toughness, K_c, is calculated as $K_c = \sqrt{2} \cdot \gamma \cdot E$, where E is the Young's modulus and γ is the surface energy, which for gelatin is equal to $1\,\mathrm{J \cdot m^{-2}}$ [*Kavanagh et al.*, 2013]. Since $G = E/2(1+\nu)$, and gelatin Poisson's ratio $\nu \sim 0.5$, we obtain $K_c = 59 \pm 2\,\mathrm{Pa \cdot m^{1/2}}$. The density $\rho \sim 1000\,\mathrm{kg \cdot m^{-3}}$ has been measured with a standard pycnometer.

The air injected at the base of the model creates a Weertman crack [*Weertman*, 1971], a laboratory analog for a dike [e.g., *Rivalta et al.*, 2015]. Propagating air-filled cracks may better apply to low-viscosity intrusions, as the dike has a thin tail and detaches from its source soon after injection. We estimate the average overpressure of the analog dikes using the formula for a Weertman crack. Such estimate may differ from the overpressure of a dike in nature if the dike is hydraulically connected to a magma chamber with overpressure on the order of $(\Delta\rho g L_z)/4$ or greater. In such case, the overpressure of the magma chamber should be considered, and the Weertman crack formula would provide the additional overpressure built up in the dike head. In the following, we will scale our experiment to nature considering a buoyant magmatic dike detached from the magma chamber or connected to a magma chamber with overpressure much smaller than $(\Delta\rho g L_z)/4$.

The length scaling factor, L^*, is set assuming that the critical buoyancy length, that is the length over which magma buoyancy driving ascent balances resistance from the host medium, must be the same in nature and in the experiment [*Kavanagh et al.*, 2013]. L^* is calculated as

$$L^* = (K_c{}^*/\Delta\rho^*)^{2/3} \quad (1)$$

where the asterisk denotes the model to nature ratio. Assuming that K_c and $\Delta\rho$ in nature are on the order of $100\,\mathrm{MPa \cdot m^{1/2}}$ [*Rivalta and Dahm*, 2006; *Rivalta et al.*, 2015] and $100\,\mathrm{kg \cdot m^{-3}}$, respectively, we obtain $L^* \sim 1 \times 10^{-5}$; therefore, 1 cm in the model is equivalent to ~1 km in nature. Since our edifice analog is 5 cm high and our dike analogs were injected at a depth of 10 cm, this corresponds to dikes injected at depth ~10 km below a volcanic edifice ~5 km high in nature.

As for the scaling of the forces, ascending analog dikes are driven by buoyancy and subject to loading forces from the volcanic edifice. The lengths of the analog dikes, and in turn their buoyancy force, are controlled by

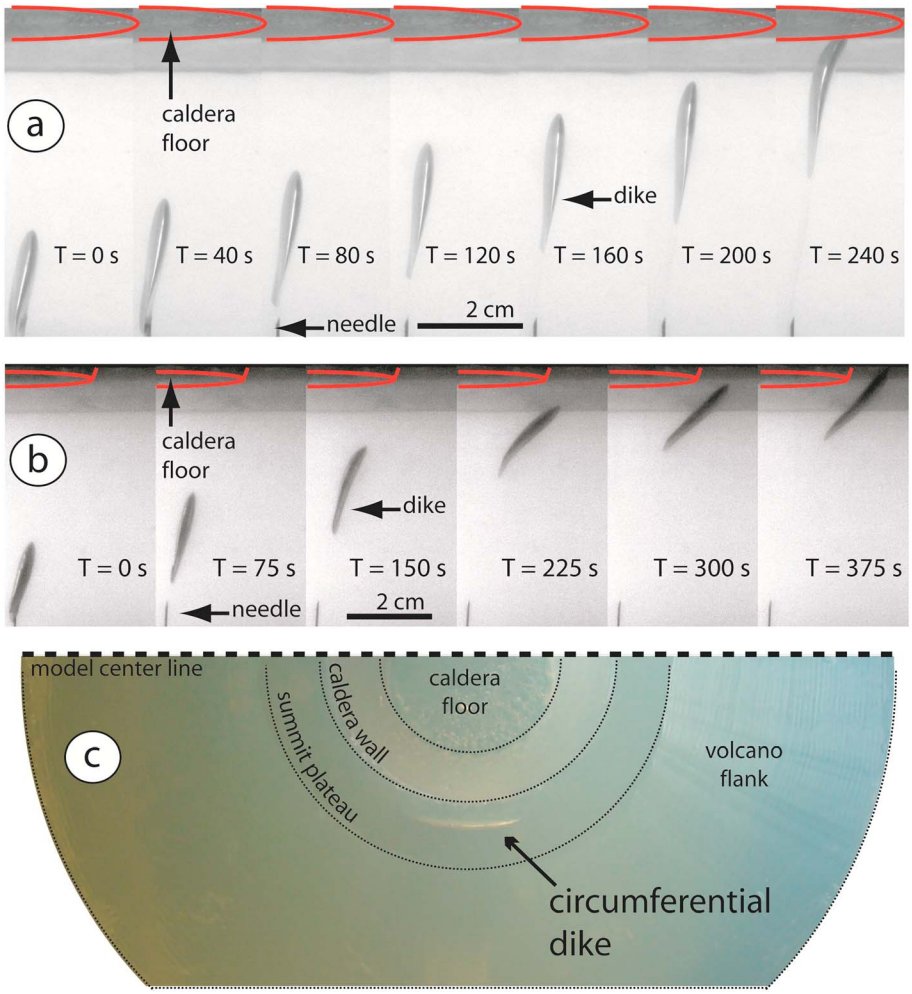

Figure 2. Time series of digital photographs showing a (a) vertically propagating dike erupting in the caldera region and a (b) deflected and arrested dike. The time interval *T* is indicated in each plot. (c) Top view photo of a circumferential dike erupting in the summit plateau region.

the volume of injection, on the order of a few cubic centimeter. In order to scale the intensity of the imposed loading/unloading (weight of the volcano cone and missing weight in the caldera), the ratio of the loading/unloading pressures to the buoyancy of the dikes, p^*, needs to be the same in nature as in the experiment:

$$p^* = (\rho_h^*\ H^*)/(\Delta\rho^*\ L^*) \tag{2}$$

where ρ_h is the density of the host medium (rock or gelatin) and H is the caldera depth. For a host rock density of 2800 kg · m^{-3}, the pressure change due to a missing volume of depth 4.5 cm in laboratory is equivalent to a 150 m of rock in nature. Note that in nature we may have an additional overpressure provided by the magma chamber that would effectively lower the denominator ($\Delta\rho^*\ L^*$).

Dimensionless parameters (e.g., ν) scale with a factor of 1 [e.g., *Hubbert*, 1937]; as a consequence the materials adopted in the models must have the same properties as in nature. The gelatin Poisson's ratio ν is 0.5 [e.g., *Takada*, 1990] while for igneous rocks ν~0.25 [e.g., *Turcotte and Schubert*, 2002]. The implications due to this discrepancy are explained in section 4.1.

3. Results

Four models where the dikes are injected below the caldera center summarize our experimental results. Similar to previous studies [e.g., *Takada*, 1990], the initial injection phase comprises the creation of a penny-shaped

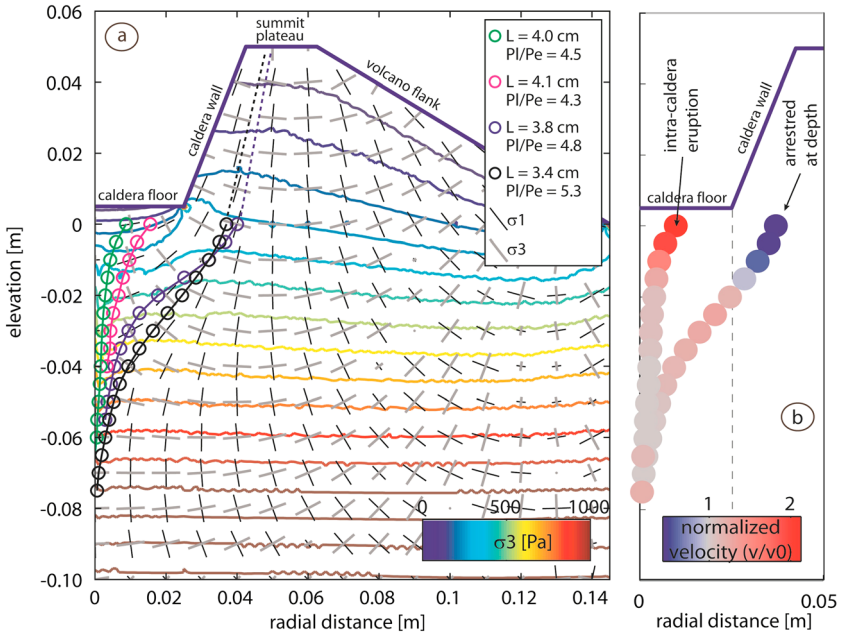

Figure 3. (a) Combination between numerical (stress orientations) and analogue data (path of analog dikes). The blue line represents the cross-sectional topography of the analog model. The open circles represent the position of the dike tip during the propagation. The dashed part of the trajectories is constrained by the eruption position in the analog model. The color coding refers to the length and overpressure of the dikes. The contour refers to the amplitude of σ_3. The directions of σ_1 and σ_3 are shown as black and gray lines, respectively. (b) Normalized propagation velocity v/v_0 (where v_0 is equal to velocity at depth) of the dikes with the innermost ($P_e/P_l = 4.5$) and outermost ($P_e/P_l = 5.3$) trajectories.

crack. Upon additional air injection the crack evolves to an elliptical form at the upper part and nearly flat tail in front view and an inverse teardrop shape in side view (Figures 2a and 2b). When the critical buoyancy length $L_b = (K_c/\Delta\rho g)^{2/3}$ ($L_b = 3.3$ cm under these experimental conditions) is reached, the crack propagates with an initial approximately constant velocity to the model surface. The analog dikes followed two distinct behaviors:

Behavior A: intracaldera eruptions. The analog dikes ascend approximately vertically from their injection point to ~1.5 cm from the caldera floor. Their final stage of propagation is characterized by a small outward deflection (~20°) from the vertical axis and by a consequent eruption within the caldera floor (Figure 2a).

Behavior B: summit plateau eruptions. Compared to behavior A, the analog dikes are subject to a more pronounced outward deflection (~35°) from the vertical axis soon after their initial propagation. This deviation allows the dike to propagate beyond the caldera rim (Figure 2b) but is accompanied by the progressive slowing down and arrest of the dike. Upon additional air injection, the dike continues to propagate, straightening up and erupting along the caldera rim as a summit circumferential fissure (Figure 2c).

Together with directional (geometric) variations, our analog dikes experience also velocity (kinematic) variations, here expressed as v/v_0, where v is the observed velocity in a given segment and v_0 is the initial propagation velocity (after the dike leaves the needle; Figure 3b). The propagation velocity at depth > ~3 cm from the caldera floor is constant and similar for all the experiments (~0.3 mm/s). At shallower depths, "behavior A" dikes accelerate up to v/v_0~2 before the eruption. "Behavior B" dikes also experience an initial acceleration ($v/v_0 = 1.2$), even at larger depths than behavior A dikes (i.e., between 2 cm and 4 cm); however, soon after the crack tip reach the inner caldera rim, they decelerate and arrest.

In hydrostatic conditions, such as in a gelatin container with flat topography, the dikes ascend vertically, without deflection [e.g., *Takada*, 1990; *Rivalta and Dahm*, 2006]. In our experiments, the hydrostatic condition is modified by the topographic load. Such perturbation creates a rotation of the principal stresses that deflects the dikes from vertical ascent [*Lawn*, 1993]. The ascending dikes experience a variable degree of deflection (Figure 3a). Low-buoyancy dikes follow closely the numerically calculated trajectory, while high-buoyancy dikes require longer distance to rotate, similar to the experimental results of *Menand et al.* [2010]. The amount of deflection is controlled by the competition between dike overpressure, P_e, and the perturbation induced

by the topographic load, P_l [*Watanabe et al.*, 2002]. P_l is equal to ρgH, where ρ is the density, g is the acceleration due to gravity, and H is the effective thickness of the surface mass change (i.e., 4.5 cm in our models). P_e is equal to $\Delta\rho g L_z/4$, where L_z is the vertical projection of the dike length and $\Delta\rho$ is the density contrast between solid and fluid. Aiming to quantify such competition between P_e and P_l on dike trajectories, we compare the observed fluid pathways with the direction of the principal stress components calculated with the Structural Mechanics module of COMSOL Multiphysics®. We generate a model that mimics the laboratory experiments. We assume a homogeneous elastic medium with 2-D axisymmetric configuration. We simulate the Plexiglas® container of the gelatin by setting no-displacement boundary conditions for both the bottom and the side of the model. The model surface is set as free, and gravity is considered to mimic the laboratory conditions so that the stresses include the load of the gelatin itself. For the subdomains we use the same parameters as the gelatin: $\rho = 1000\ \mathrm{kg \cdot m^{-3}}$, $\nu = 0.499$, and $G = 580$ Pa.

The numerical models show that at the center of the gelatin container and at depth larger than 6 cm σ_3 is subhorizontal (Figure 3a). All the dikes follow the modeled stress patterns (i.e., they propagate vertically). Moving toward the surface, σ_3 rotates progressively becoming subvertical just beneath the caldera floor. This is consistent with the outward deflection that the analog dikes undergo during their ascent. Dikes that erupt within the caldera floor (i.e., high-overpressure dikes with $P_l/P_e = 4.3$–4.5) proceed almost insensitive to the stress rotation at depth $<$2–3 cm, with a marked mismatch (up to 80°) between observed trajectory and σ_1 (see Figure S1 in the supporting information). Conversely, when $P_l/P_e = 4.8$–5.3 the analog dikes closely follow the direction of σ_1. The potential interaction with a pressurized magma chamber (which is neglected in our calculation and in our analog models) may increase the initial dike overpressure (lowering P_l/P_e) and may affect the initial orientation of the dike (because of the reservoir-induced stresses). However, during the dike growth, the reservoir pressure will decrease, so that its effect on the dike propagation path is expected to progressively vanish. Our stress calculation also indicates that σ_3 is always lying on the axisymmetric plane, consistently with the exclusive observation of circumferential fissures during the experiments.

4. Discussion and Conclusions

4.1. The Stress State of a Volcano with Summit Caldera: Models Versus Nature

Our analog and numerical models quantify the unbuttressing effect of a caldera on the stresses on the caldera rim [e.g., *Munro and Rowland*, 1996], where a radially oriented σ_3 is consistent with proximal circumferential dikes and fissures. Our models illustrate this effect for an end-member stress state, where the volcano is subject to gravitational loading, a condition applicable to volcanic edifices where the growth of the edifice and gravitational loading within the edifice is not compensated by stress-homogenizing inelastic effects such as diking or fracturing. In nature, repeated dike injections and fracturing may progressively reduce the deviatoric stresses in favor of an isotropic condition [*Chadwick and Dieterich*, 1995]. The effect of a caldera on an isotropically stressed volcano is that of orienting σ_3 radially at proximal distance and circumferentially beneath the flanks [*Corbi et al.*, 2015]. In both the gravitationally loaded and in the isotropically stressed cases, a summit caldera has thus the effect of deflecting ascending dikes and, in case of relatively shallow sources, eventually focusing them along the caldera rim as circumferential fissures.

Additional insight emerges from the comparison between the analog and numerical models. First, we show that the principal stress orientations depend on Poisson's ratio and dimensions of the gelatin container R_b (Figure 4). As mentioned above, gelatin has higher incompressibility with respect to rocks, therefore not fully satisfying the scaling requirements. Aiming to quantify this discrepancy, we generate an additional numerical model similar to that described above but with $\nu = 0.25$ (Figure 4b). In addition, we test the potential wall effect due to the container by producing an additional numerical model doubling the size of the container (i.e., $R_b = 30$ cm; Figure 4c). Below the caldera rim σ_3 is subhorizontal and within the axisymmetric plane for all models. This confirms that (a) the vertical circumferential dikes observed below the caldera rim in our analog models represent a solid and reproducible feature despite the host rock analog incompressibility and the relatively small box, (b) the gelatin models represent a good analog when modeling circumferential dikes in a gravitationally loaded condition, and (c) a larger container is necessary to model the stress in the entire edifice. We obtained circumferential fluid-filled fractures in gelatin, in contrast to what previously predicted for strong, cohesive media, including gelatin itself [*Galland et al.*, 2014]. We suggest that circumferential dikes in strong, cohesive media can occur if σ_3 is radially oriented, e.g., due to magma chamber stresses

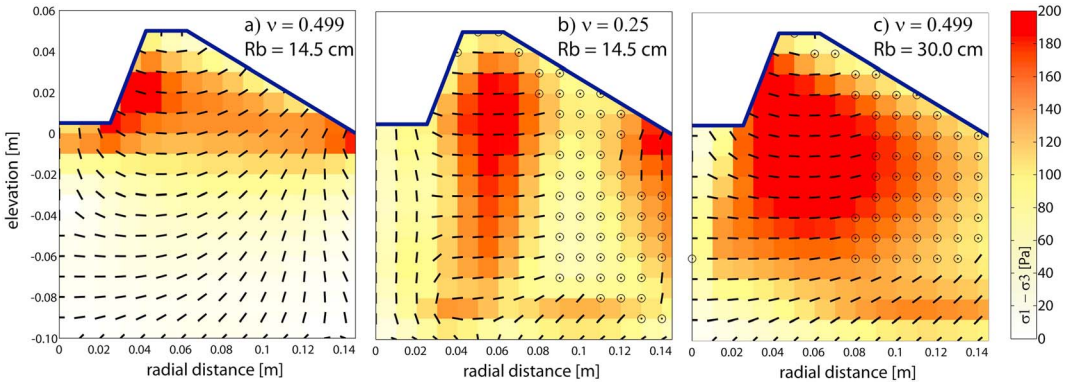

Figure 4. Comparison of the orientation of σ_3 (black lines) within the gelatin for a model with (a) $\nu = 0.499$ and $R_b = 14.5$ cm, (b) $\nu = 0.25$ and $R_b = 14.5$ cm, and (c) $\nu = 0.499$ and $R_b = 30$ cm. The black circles are used to indicate σ_3 out of the axisymmetric plane. The background shading highlights the differential stress σ_1-σ_3. The blue lines represent the cross-sectional topography of the analog model.

[e.g., *Chadwick and Dieterich*, 1995] or, as shown here, due to the presence of a caldera. Below the caldera floor the model with $\nu = 0.25$ has subvertical σ_3 from the bottom of the container to the surface, similar to the shallowest 4 cm of the model with $\nu = 0.499$, and compatible with sill geometry. Such sill-like structures seem to be a common feature beneath caldera floors in nature, as for example at Fernandina (Galapagos [*Bagnardi et al.*, 2013]), Campi Flegrei (Italy [*D'Auria et al.*, 2015]), and Toba (Sumatra [*Jaxybulatov et al.*, 2014]). Large discrepancies in the stress orientations are found beneath the volcano flanks, where the model with $\nu = 0.25$ (Figure 4b) and the model with $R_b = 30$ cm (Figure 4c) show σ_3 out of plane, suggesting a radial dike arrangement similar to nature [e.g., *Acocella and Neri*, 2009].

We conclude that the stress pattern within the gelatin should be verified with numerical models aiming to test if a feature observed in the analog models is robust or just an artifact due to gelatin incompressibility or boundary effects, and if this is the case, a larger box or different analog material with lower ν may be necessary for properly modeling dike orientation in laboratory.

4.2. Kinematics of Dike Ascent and Implications for the Development of Circumferential Fissures

In addition to the information on the magma pathway that can be obtained to a large extent from numerical models, here we also obtain information on the kinematics of dike ascent in 3D. This represents the greatest advantage of experiments with respect to numerical models. In fact, at the current state of the art those numerical models that are able to provide information on dike kinematics taking into account the stress heterogeneities [e.g., *Pinel and Jaupart*, 2000] do not provide any information on magma path, whereas numerical models able to predict dike trajectories cannot account for dike kinematics [e.g., *Rivalta et al.*, 2015].

Our experiments show two different behaviors depending on dike buoyancy: (a) if the dike is buoyant (i.e., long and with low-density magma), it will reach the surface within the caldera, being affected by the free surface lately, and (b) if the dike is less buoyant (i.e., short and with dense magma), it will be deflected, feel the free surface at greater depth, and be arrested below the caldera rim. In analogy with previous experiments performed in plane strain geometry [*Watanabe et al.*, 2002], we found that when $P_l/P_e \sim 5$, the deflection capacity reaches its maximum and dikes propagate closely orthogonal to σ_3. Dikes erupting within the caldera floor experience a gradual acceleration at shallow depth (~2 cm). Such acceleration is due to the free surface effect [*Rivalta and Dahm*, 2006]. A similar acceleration episode has been documented during the 1998 eruption at Piton de la Fournaise, where the hypocenter migration increased from ~2 km/d 3 to 1 day before the eruption to ~11 km/d a few hours before the eruption [*Battaglia*, 2001]. Our experiments also show dikes that slow down and arrest below the caldera floor. These effects are particularly evident for low-buoyancy dikes. The slowing down phase is preceded by a small acceleration that occurs at larger depths, as low-buoyancy dikes are more sensitive to the free surface [*Rivalta and Dahm*, 2006]. The slowing down and arrest of these dikes occur as soon as they reach the caldera floor as they are subject to a rapid increase of the loading condition that tends to inhibit the propagation (Figure 2b). This observation highlights that the caldera side acts as a trap for deeper magma, as these intrusions may remain confined below

the rim. This suggest that most dikes ascending from below the caldera will preferentially be stored in the system as subhorizontal intrusions or cone sheets rather than directly erupt, explaining why circumferential dikes are observed very frequently in eroded systems while circumferential fissures at the surface are rare. The subsurface structure of calderas may also influence dike propagation. In fact, dikes within the caldera may became both arrested at the ring fault or deflected up along the fault to form a circumferential dike which may reach the surface [*Browning and Gudmundsson*, 2015].

Beside a weak tectonic stress that does not mask the effect of the presence of the caldera [*Corbi et al.*, 2015], the formation of circumferential fissures requires that the dike overpressure is initially low: in this way the dikes follow closely the trajectories defined by the ambient stresses and become shallow dipping below the caldera or deviate to the rim. A late-stage incremental overpressure through repeated supply of magma will activate the sill and drive the nucleated dike to erupt. Therefore, low-buoyancy and low-viscosity magma with regular supply from below is the ideal candidate to feed circumferential fissure eruptions. High-viscosity intrusions are less mobile and require strong source pressure to propagate large distances. This may explain why circumferential fissures mostly occur in basaltic caldera volcanoes with clear topographic evidence and continuous supply from the magma reservoir. The evidence that circumferential fissures have been witnessed in the well-defined basaltic calderas in the western Galapagos [*Chadwick and Howard*, 1991], with repeated recent eruptions, supports our modeling results. On the other hand, felsic cone sheets arrested before eruption are found in eroded systems as for example at La Gomera (Canary island [*Ancochea et al.*, 2003]) and partly at Otoge igneous complex (central Japan [*Geshi*, 2005]) and more rarely feed circumferential fissures as for example at Rano Kau (Easter Island, SE Pacific [*Vezzoli and Acocella*, 2009]). Our results thus contribute defining the shallow magma transfer below the rim of felsic and mafic calderas and why circumferential fissures are most likely fed by mafic magma.

Acknowledgments

We thank the Editor Andrew Newman, the Associate Editor, and the reviewers Nicolas Le Corvec, Steffi Burchardt and Thierry Menand who helped in improving this manuscript with their constructive comments. The research leading to these results has received funding from the European Research Council under the European Union's Seventh Framework Program (FP/2007–2013)/ERC grant agreement 240583. Experiments were performed at Laboratory of Experimental Tectonics (Università Roma Tre). Both the analog and numerical model data shown in Figures 3 and 4 are available by contacting the corresponding author.

References

Acocella, V., and A. Tibaldi (2005), Dike propagation driven by volcano collapse: A general model tested at Stromboli, Italy, *Geophys. Res. Lett.*, *32*, L08308, doi:10.1029/2004GL022248.

Acocella, V., and M. Neri (2009), Dike propagation in volcanic edifices: Overview and possible developments, *Tectonophysics*, *471*(1–2), 67–77, doi:10.1016/j.tecto.2008.10.002.

Ancochea, E., J. L. Brändle, M. J. Huertas, C. R. Cubas, and F. Hernan (2003), The felsic dikes of La Gomera (Canary Islands): Identification of cone sheet and radial dike swarms, *J. Volcanol. Geotherm. Res.*, *120*, 197–206.

Anderson, E. M. (1951), *The Dynamics of Faulting and Dyke Formation with Applications in Britain*, 2nd ed., pp. 206, Oliver and Boyd, London.

Bagnardi, M., F. Amelung, and M. P. Poland (2013), A new model for the growth of basaltic shields based on deformation of Fernandina volcano, Galápagos Islands, *Earth Planet. Sci. Lett.*, *377–378*, 358–366.

Battaglia, J. (2001), Quantification sismique des phenomenes magmatiques sur le Piton de la Fournaise entre 1991 et 2000, PhD thesis, Universite Paris 7, Denis Diderot.

Browning, J., and A. Gudmundsson (2015), Caldera faults capture and deflect inclined sheets: An alternative mechanism of ring dike formation, *Bull. Volcanol.*, doi:10.1007/s00445-014-0889-4.

Burchardt, S., and A. Gudmundsson (2009), The infrastructure of Geitafell Volcano, Southeast Iceland, in *Studies in Volcanology: The Legacy of George Walker*, *Special Publications of IAVCEI 2*, edited by T. Thordarson et al., pp. 349–370, Geological Society, London.

Burchardt, S., V. R. Troll, L. Mathieu, H. C. Emeleus, and C. H. Donaldson (2013), Ardnamurchan 3D cone-sheet architecture explained by a single elongate magma chamber, *Sci. Rep.*, *3*, 2891.

Chadwick, W. W., and J. H. Dieterich (1995), Mechanical modeling of circumferential and radial dike intrusion on Galapagos volcanoes, *J. Volcanol. Geotherm. Res.*, *66*(1–4), 37–52, doi:10.1016/0377-0273(94)00060-T.

Chadwick, W. W., and K. Howard (1991), The pattern of circumferential and radial eruptive fissures on the volcanoes of Fernandina and Isabela Islands, Galapagos, *Bull. Volcanol.*, *53*, 259–275.

Chestler, S. R., and E. B. Grosfils (2013), Using numerical modeling to explore the origin of intrusion patterns on Fernandina volcano, Galapagos Islands, Ecuador, *Geophys. Res. Lett.*, *40*, 4565–4569, doi:10.1002/grl.50833.

Corbi, F., E. Rivalta, V. Pinel, F. Maccaferri, M. Bagnardi, and V. Acocella (2015), How caldera collapse shapes the shallow emplacement and transfer of magma in active volcanoes, *Earth Planet. Sci. Lett.*, *431*, 287–293, doi:10.1016/j.epsl.2015.09.028.

D'Auria, L., B. Massa, E. Cristiano, C. Del Gaudio, F. Giudicepietro, G. Ricciardi, and C. Ricco (2015), Retrieving the stress field within the Campi Flegrei caldera (southern Italy) through an integrated geodetical and seismological approach, *Pure Appl. Geophys.*, *172*(11), 3247–3263, doi:10.1007/s00024-014-1004-7.

Dahm, T. (2000), Numerical simulations of the propagation path and the arrest of fluid-filled fracture in the Earth, *Geophys. J. Int.*, *141*, 623–638.

Di Giuseppe, E., F. Funiciello, F. Corbi, G. Ranalli, and G. Mojoli (2009), Gelatins as rock analogs: A systematic study of their rheological and physical properties, *Tectonophysics*, *473*(3–4), 391–403, doi:10.1016/j.tecto.2009.03.012.

Fiske, R. S., and E. D. Jackson (1972), Orientation and growth of Hawaiian volcanic rifts: The effect of regional structure and gravitational stresses, *Proc. R. Soc. Lond.*, *329*, 299–326.

Galland, O., S. Burchardt, E. Hallot, R. Mourgues, and C. Bulois (2014), Dynamics of dikes versus cone sheets in volcanic systems, *J. Geophys. Res. Solid Earth*, *118*, 6178–6192, doi:10.1002/2014JB011059.

Geshi, N. (2005), Structural development of dike swarms controlled by the change of magma supply rate: The cone sheets and parallel dike swarms of the Miocene Otoge igneous complex, central Japan, *J. Volcanol. Geotherm. Res.*, *141*(3–4), 267–281, doi:10.1016/j.jvolgeores.2004.11.002.

Gudmundsson, A. (2006), How local stresses control magma-chamber ruptures, dyke injections, and eruptions in composite volcanoes, *Earth Sci. Rev.*, *79*(1–2), 1–31, doi:10.1016/j.earscirev.2006.06.006.
Hooper, A., B. Ófeigsson, F. Sigmundsson, B. Lund, P. Einarsson, H. Geirsson, and E. Sturkell (2011), Increased capture of magma in the crust promoted by ice-cap retreat in Iceland, *Nat. Geosci.*, *4*(11), 783–786, doi:10.1038/ngeo1269.
Hubbert, M. K. (1937), Theory of scale models as applied to the study of geologic structures, *Geol. Soc. Am. Bull.*, *48*, 1459–1520.
Jaxybulatov, K., N. M. Shapiro, I. Koulakov, and A. Mordret (2014), A large magmatic sill complex beneath the Toba caldera, *Science*, *346*, 617, doi:10.1126/science.1258582.
Kavanagh, J. L., T. Menand, and K. A. Daniels (2013), Gelatine as a crustal analogue: Determining elastic properties for modelling magmatic intrusions, *Tectonophysics*, *582*, 101–111, doi:10.1016/j.tecto.2012.09.032.
Lawn, B. (1993), *Fracture of Brittle Solids*, 2nd ed., pp. 378, Cambridge Univ., Cambridge.
Maccaferri, F., M. Bonafede, and E. Rivalta (2011), A quantitative study of the mechanisms governing dike propagation, dike arrest and sill formation, *J. Volcanol. Geotherm. Res.*, *208*(1–2), 39–50, doi:10.1016/j.jvolgeores.2011.09.001.
Maccaferri, F., E. Rivalta, D. Keir, and V. Acocella (2014), Off-rift volcanism in rift zones determined by crustal unloading, *Nat. Geosci.*, *7*, 297–300, doi:10.1038/NGEO2110.
Maccaferri, F., V. Acocella, and E. Rivalta (2015), How the differential load induced by normal fault scarps controls the distribution of monogenic volcanism, *Geophys. Res. Lett.*, *42*, 7507–7512, doi:10.1002/2015GL065638.
Menand, T., K. Daniels, and P. Benghiat (2010), Dyke propagation and sill formation in a compressive tectonic environment, *J. Geophys. Res.*, *115*, B08201, doi:10.1029/2009JB006791.
Munro, D. C., and S. K. Rowland (1996), Caldera morphology in the western Galapagos and implications for volcano eruptive behavior and mechanisms of caldera formation, *J. Volcanol. Geotherm. Res.*, *72*, 85–100.
Pinel, V., and C. Jaupart (2000), The effect of edifice load on magma ascent beneath a volcano, *Philos. Trans. R. Soc. A Math. Phys. Eng. Sci.*, *358*(1770), 1515–1532.
Rivalta, E., and T. Dahm (2006), Acceleration of buoyancy-driven fractures and magmatic dikes beneath the free surface, *Geophys. J. Int.*, *166*(3), 1424–1439, doi:10.1111/j.1365-246X.2006.02962.x.
Rivalta, E., B. Taisne, A. P. Bunger, and R. F. Katz (2015), A review of mechanical models of dike propagation: Schools of thought, results and future directions, *Tectonophysics*, *638*, 1–42, doi:10.1016/j.tecto.2014.10.003.
Roman, A., and C. Jaupart (2014), The impact of a volcanic edifice on intrusive and eruptive activity, *Earth Planet. Sci. Lett.*, *408*, 1–8, doi:10.1016/j.epsl.2014.09.016.
Sigmundsson, F., et al. (2015), Segmented lateral dyke growth in a rifting event at Bárðarbunga volcanic system, Iceland, *Nature*, *517*(7533), 191–195, doi:10.1038/nature14111.
Takada, A. (1990), Experimental study on propagation of liquid-filled crack in gelatin: Shape and velocity in hydrostatic stress condition, *J. Geophys. Res.*, *95*(B6), 8471–8481, doi:10.1029/JB095iB06p08471.
Turcotte, D. L., and G. Schubert (2002), *Geodynamics*, 2nd ed., 456 pp., Cambridge Univ. Press, Cambridge, New York.
Vezzoli, L., and V. Acocella (2009), Easter Island, SE Pacific: An end-member type of hotspot volcanism, *Geol. Soc. Am.*, *121*(5), 869–886, doi:10.1130/B26470.1.
Watanabe, T., et al. (2002), Analog experiments on magma-filled cracks: Competition between external stresses and internal pressure, *Earth Planets Space*, *54*, 1247–1261.
Weertman, J. (1971), Theory of water-filled crevasses in glaciers applied to vertical magma transport beneath oceanic ridges, *J. Geophys. Res.*, *76*, 1171–1183, doi:10.1029/JB076i005p01171.